Speed Sensorless Vector Controlled Induction Motor Drive Using Single Current Sensor

K.Vinodh kumar [1], K.C.Satheesh [2], S.Nagaraju[3]
[1, 2, 3] Dept of EEE
[1, 2, 3] SIT,Puttur.

Abstract- *New speed and current estimation techniques are pro-posed in this paper. These are used to formulate a single current sensor-based vector controlled drive. The speed sensorless control is formulated by developing a new model reference adaptive system (MRAS) using the outer product of v_s and i_s as the functional candidate. Contrary to the method available that depends on sta-tor resistance, the proposed approach is immune to the variation of stator resistance. This is possible by using reference quantities (i.e., voltage and currents) in reference model and actual quanti-ties (i.e., currents) in adjustable model. The current estimation on the other side extracts the information of the phase currents in two-phase stationary reference frame by using the corresponding synchronous reference frame variables and the vector rotator. The current estimation also does not depend on stator resistance and hence the complete system can perform very well at low speed. The proposed speed and current estimation techniques are simu-lated in MATLAB/Simulink and experimentally validated through a dSPACE-1104-based laboratory prototype.*

I. INTRODUCTION

INDUCTION motor (IM) drives are extensively used in in-dustry due to their cost effectiveness, ruggedness and low maintenance requirements. Field-oriented-controlled or vector-controlled drive has become an industry standard for high-performance applications. Speed, current, and/or volt-age sensors are usually required in vector controlled drives. Rotor speed information is necessary for speed-controlled sys-tem. The fast current controller operates in the inner current loop and a slower speed controller stays in the outer speed loop to generate the corresponding reference currents for the current controllers. Efforts are put to reduce the number of sensors by signal estimation/processing. Single-sensor-based vector-controlled drives have the unique advantage of lowest cost and size. Only a few publications are available on this topic . This paper deals with a single current sensor-based controller eliminating the speed sensor and one of the two current sensors those are required in standard drives. A brief literature survey on the different types of speed and current estimation strate-gies is first presented followed by a discussion on the proposed controller in this section.

Elimination of the speed sensor makes the drive mechan-ically more robust. Different techniques have been proposed to estimate speed for IM drives and . Such approaches are broadly divided into model-based and signal-injection-based methods. Of the model-based techniques, model reference adaptive system (MRAS) is successfully applied for speed estimation. Flux, back-emf, reactive power, etc., are used to form the MRAS. Presence of pure integrator and dependency on stator resistance are the limitations of flux-based MRAS.

MRAS using back-emf as the functional candidate overcomes the pure integration problem but at the cost of introducing derivative terms. The system also involves stator resistance . Reactive-power-based MRAS is one of the alternatives that does not involve stator resistance and is very suitable for low-speed operation. Also, the absence of pure integrator makes such approach useful for practical systems with dc offset and noise. However, such technique is found to be unstable in regenerative mode.

Instability under regenerative mode is one of the key issues for adaptive speed sensorless IM drives. Extensive efforts are put to improve the stability of such systems . Full order as well as reduced order observers are proposed and different algo-rithms to tune the adaptive gains have been reported. Further improvements in performance are attempted by includ-ing current-integral and modified statically compensated voltage model .A unique approach to ensure complete sta-bility through determination of the gains of the reduced order observer is also reported , Under the assumption of fast sta-tor current dynamics, the gain selections of full order observers are also found. Thus, a framework to compare the performance of different full- and reduced-order observers is achieved .

Investigations to improve the stability of MRAS-based drive in all the four quadrants are also reported in literature. The problem of instability in regenerative mode for a reactive-power-based MRAS is solved with the help of artificial neural network (ANN) . In a recent paper , an X-based MRAS is pro-posed which is stable in all the four quadrants of operation. Dependency on stator resistance

restricts performance of such system at low speed. A modified X-MRAS is proposed here to overcome the dependence on stator resistance.

In an extreme case, the speed sensorless drive may be de-signed to operate with only one current sensor, where the speed and the second current sensor are replaced by the corresponding estimated signals. In addition, adopting a single current sen-sor is more cost effective. A few single current sensor-based speed estimation techniques have been proposed in the litera-ture Generally, the three-phase line currents are re-constructed from the dc-link current and switching states of the inverter. A review on various estimation methods based on dc-link current measurement is presented in . The issues re-lated to the reconstruction of phase current from dc-link current measurement are: 1) low modulation index; 2) short duration of active voltage vector; 3) protection against different fault conditions; and 4) phase shift in reconstructed current signals. The first limitation is overcome in where a single current sensor is used to measure a phase current and a branch current simultaneously. The second limitation can be overcome by mea-surement vector insertion method (MVIM) . Protection of such systems is also reported . Three individual observers (one for each phase) are used in to estimate phase current from voltage and flux signals. This method is dependent on the variation of stator resistance. A sinusoidal curve fitting ob-server is used in to estimate phase currents from the dc-link current. This type of observer is independent of the load pa-rameters. A jitter-like phenomenon in the reconstructed current signal (based on dc-link current measurement) and its reduc-tion have been addressed in . It is noticed that all of the aforesaid methods based on dc-link current measurement require the information of machine model and switching states of the inverter.

In this paper, a new current estimation method is presented which does not need the information of the switching states of the inverter. However, this requires unit vector, which, in turn, involves rotor time constant. Here, the current sensor is placed in any one phase of the machine terminals, instead of the dc-link. While this has the advantage of very accurately sensing the phase current; however, this is at the cost of a redundancy in inverter protection in case of shoot-through faults. Note that the inverter devices are primarily protected by sensing the collector-emitter voltage, when the switch is ON (i.e., by $V_{C\ E\ sa\ t}$ protection). The proposed current estimation method requires the information of rotor speed, which is derived from an X-MRAS. A specially constructed X-MRAS is used in this paper. The reference and adjustable model of modified X-MRAS are computed in rotat-ing reference frame. Both of the speed and current estimation methods are independent of stator resistance variation.

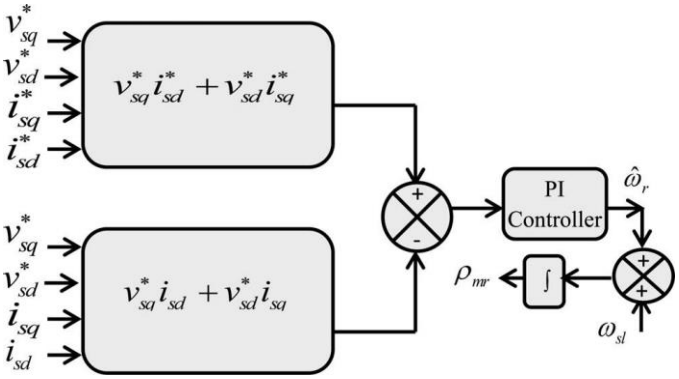

Fig. 1. Structure for speed estimation.

The paper is divided into seven sections. Section I deals with literature review on various speed and current estimation tech-niques. The proposed speed and current estimation algorithms are discussed in Sections II and III, respectively. Simulation and experimental results are presented in Sections IV and VI, re-spectively. Section V deals with the experimental setup. Finally, Section VII concludes the work.

II. PROPOSED SPEED ESTIMATION ALGORITHM

The speed is estimated using the concept of MRAS, where a reference and an adjustable model compute a certain system variable (in literature this is known as functional candidate). The system variable computed by the reference model does not depend on the quantity to be estimated, whereas the adjustable model depends directly or indirectly on the estimated quantity. Like P and Q, here a fictitious (i.e., has no physical existence)quantity, termed as X ($X = v_s\ i_s$) is considered as the func-tional candidate. The quantity X in reference model (X_r) is computed using the reference values of voltages and currents. The same value of X in adjustable model (X_a) is computed with the help of reference values of voltages and actual cur-rents. The actual values of *d*- and *q*-axis currents are obtained by transforming two-phase currents (i.e., $i_{s\ \alpha}$ and $i_{s\ \beta}$) with the help of vector rotator (which, in turn, depends on speed). The signal $i_{s\ \beta}$ is obtained from the current estimation algorithm, as described in Section III. The structure of the speed estimation algorithm is shown in Fig. 1. The reference model computes X_r using the controller generated command signals and hence does not require the information of rotor speed. On the contrary, (3) shows that the expression of X_a involves rotor speed, as $\rho_{m\ r}$ is computed using (4).

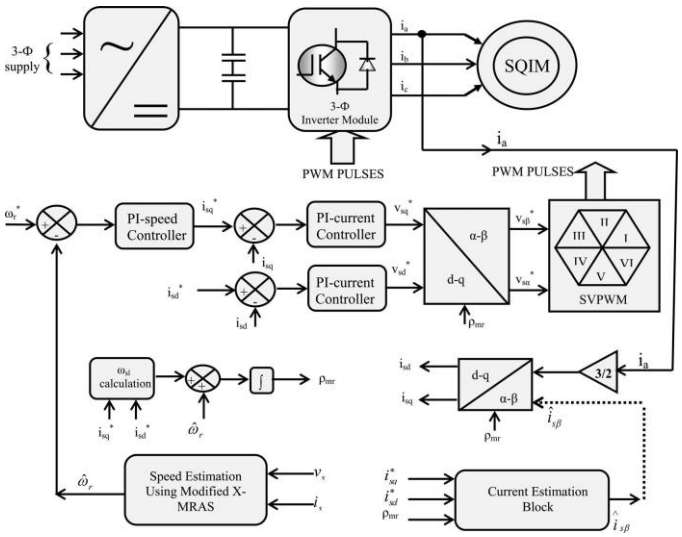

Fig. 2. Schematic block diagram of IM drive with modified X-MRAS and proposed current estimation technique.

$$X_t = v^*_{sq}\, i^*_{sd} + v^*_{sd}\, i^*_{sq} \quad (1)$$

$$X_a = v^*_{sq}\, i_{sd} + v^*_{sd}\, i_{sq} \quad (2)$$

or,

$$X_a = v^*_{sq}\, i_{s\alpha}\, e^{-j\rho_{mr}} + v^*_{sd}\, i_{s\beta}\, e^{-j\rho_{mr}} \quad (3)$$

$$\rho_{mr} = \omega_e\, dt \quad (4)$$

where $\omega_e = \hat{\omega}_r + \omega_{sl}$.

III. PROPOSED CURRENT ESTIMATION ALGORITHM

In the proposed controller, the speed and one of the currents need to be estimated as the system runs with only one current sensor. The speed estimation also requires an estimate of the current. This section first deals with several current estimation methods reported in the literature and then present the proposed urrent estimation technique.

Green and Williams proposed the reconstruction of phase currents from the dc-link current signal in 1989. Reference and introduced modifications to the modulation algorithm in order to guarantee the reliability of the measurements from the dc-link current sensors. Motor phase current was also estimated by using prediction–correction algorithms, thus introducing additional computational burden to the drive system .

In , a space vector modulation pattern modification (SVM-PM) is proposed that produces lower current harmonic content. The SVM-PM, required to reconstruct the phase currents, increments the power losses, the audible noise and the high-frequency content in voltages and current. The inverter output voltage is reduced by the SVM-PM in the over modulation operating mode. The negative effects of SVM-PM is overcome in with the help of a state observer working along with SVM-PM. In, direct torque control (DTC) scheme for IM drives based on single current sensor placed in the inverter dc-link is proposed. Here, the phase current is first predicted by means of suitable motor model and then adjusted with the help of sensed dc-link current. The drawback is the additional computational burden. Reference proposes a method and a current sensor arrangement for the acquisition of true instantaneous phase current from the dc-link signal, together with the short-circuit and ground fault protections implemented with only one current sensor. The dc-link sensed current remains sensitive to narrow-pulse problems, and further deteriorate if the cable capacitance causes spurious oscillations in the dc-link waveform. This problem is solved ,where the control algorithm is based on calculations of instantaneous active and reactive power from the dc-link current and pulsewidth-modulated (PWM) pattern. In all the aforementioned methods, current sensor is placed in the dc-link. In], single current sensor topology for matrix converter is proposed.

The proposed current estimation scheme is shown in Fig. 3. The current sensor is assumed to be placed in one of the phases (say phase-A) of the machine. The α-axis (which is oriented along the phase-A axis) current in two-phase stationary refer-ence frame is calculated using the transformation matrix given by

$$\begin{bmatrix} i_{s\alpha} \\ i_{s\beta} \end{bmatrix} = K \begin{bmatrix} 1 & \frac{-1}{2} & \frac{-1}{2} \\ 0 & \frac{-\sqrt{3}}{2} & \frac{\sqrt{3}}{2} \end{bmatrix} \begin{bmatrix} i_a \\ i_b \\ i_c \end{bmatrix}$$

where "K" is a constant. The magnitude of K is assumed to be 1 at per with the available literature [1]. Thus, we get

$$K = \frac{3}{2} \quad (5)$$

Estimation of β-axis current ($i_{s\beta}$) is carried out using the reference values of d- and q-axis currents (i.e., i^*_{sd} and i^*_{sq}). The unit vectors are also required in the current estimation. The β-axis rotor voltage in stationary reference frame is expressed as follows:

$$v_{r\beta} = R_r\, i_{r\beta} + \frac{d}{dt}\psi_{r\beta} - \omega_r\, \psi_{r\alpha} \quad (6)$$

For a squirrel-cage induction machine, $v_{r\beta} = 0$. Thus (6) can be rewritten as

$$0 = R_r i_{r\beta} + \frac{d}{dt}\psi_{r\beta} - \omega_r \psi_{r\alpha} \quad (7)$$

The equations for rotor flux in stationary reference frame are expressed as:

$$\psi_{r\alpha} = L_m i_{s\alpha} + L_r i_{r\alpha} \quad (8)$$

$$\psi_{r\beta} = L_m i_{s\beta} + L_r i_{r\beta} \quad (9)$$

Substituting the value of $i_{r\beta}$ from (9) into (7), we get

$$\frac{d}{dt}\psi_{r\beta} = \frac{L_m}{\tau_r} i_{s\beta} - \frac{\psi_{r\beta}}{\tau_r} + \omega_r \psi_{r\alpha} \quad (10)$$

Also, $\psi_{r\beta} = |\psi_r| \sin \rho_{m\,r}$ and $\psi_{r\alpha} = |\psi_r| \cos \rho_{m\,r}$. Substituting the values of $\psi_{r\alpha}$ and $\psi_{r\beta}$ into (10), we get

$$\psi_r \cos \rho_{m\,r}\, \omega_e = \frac{L_m}{\tau_r} i_{s\beta} - \frac{\psi_r \sin \rho_{m\,r}}{\tau_r} + \omega_r \psi_r \cos \rho_{m\,r} \quad (11)$$

or

$$\psi_r \cos \rho_{m\,r}\, \omega_{sl} = \frac{L_m}{\tau_r} i_{s\beta} - \frac{\psi_r \sin \rho_{m\,r}}{\tau_r} \quad (12)$$

Substituting $\omega_{sl} = (1/\tau_r)(i_{sq}^*/i_{sd}^*)$ in (12), the estimated value of the β-axis stator current can be expressed as:

$$\hat{i}_{s\beta} = \frac{1}{L_m} \frac{i_{sq}^*}{\psi_r \cos \rho_{m\,r}} + \psi_r \sin \rho_{m\,r} \quad (13)$$

Equation (13) is in general form. It involves computation of flux, unit vector along with reference d- and q-axis currents. For field-oriented drive, applying $|\vec{\psi}_r| = L_m i_{sd}^*$, (13) may further be expressed as

$$\hat{i}_{s\beta} = i_{sq}^* \cos \rho_{m\,r} + i_{sd}^* \sin \rho_{m\,r} \quad (14)$$

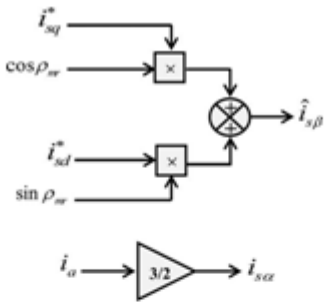

Fig. 3. Estimation of β -axis stator current.

TABLE I
MACHINE RATING AND PARAMETERS

Stator phase voltage (V)	400
Stator phase current (A)	4.4
Shaft power (kW)	1.8
Pole pairs	2
Base speed (rpm)	1370
Magnetizing inductance (mH)	670.5
Stator and rotor leakage inductance (mH)	14.3
Stator resistance (Ω)	5.71
Rotor resistance(Ω)	4.08
Rotor inertia (Kg-m^2)	0.011

The position of the rotor flux vector (ρm r) is computed ac-cording to (4). Therefore, the estimation of current requires rotor speed, which is obtained from the modified X-MRAS.The schematic block diagram of the complete system is shown in Fig. 2.

IV. SIMULATION RESULTS

The proposed single current sensor-based speed sensorless vector-controlled IM drive is simulated in MATLAB/Simulink. This section first presents the simulation results showing the robustness of current estimator when the current controller is subjected to a disturbance. Thereafter, simulation results corresponding to other operating conditions of the drive are presented. Parameters of the machine are given in Table I.

A. Performance of the Current Estimator When Subjected to a Disturbance

The performance of system for a disturbance in i^* is presented here. The drive is running under steady state with the corresponding q-axis current (i.e., I^*) of 4.05 A. At 35 s, a disturbance (Δi_{sq}) in the form of a step command is added to i^* (i.e., i_{sq} = 0.405 A). Fig. 4 shows the situation considered. The disturbance is withdrawn at 35.01 s. Thus, the system is subjected to a 10% error between reference and actual q-axis currents to study the behavior of the current estimation mechanism. The actual and estimated speeds are found to have an error of 0.1% and 0.4%. Fig. 5 shows the corresponding simulation results. Flux orientation can be observed in Fig. 5(c).

From Fig. 5(e), it can be observed that estimated value of β-axis

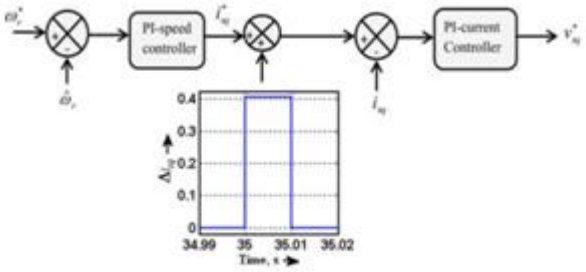

Fig. 4. Speed loop with a step disturbance (Δi_{sq}) in i^*_{sq}.

B. Step Response

A step change in speed command from 20 to 30 rad/s is applied at 20 s maintaining torque constant at 1 p.u. The actual motor speed (ω_r) under such step change is shown in Fig. 6(a). The actual (ω_r) and estimated ($\hat{\omega}_r$) speeds are presented in Fig. 6(b). The motor flux in rotor flux oriented reference frame is available in Fig. 6(c), which represents flux orientation. The q- and *d*-axis stator currents are presented in Fig. 6(d) and (e).

C. Speed Reversal in Step

The performance of the drive under speed reversal is shown in Fig. 7. The reference speed is changed from +20 to −20 rad/s at 17.5 s. The actual speed follows the reference speed [see Fig. 7(a)]. The actual and estimated speeds are illustrated in Fig. 7(b), which are found to be sufficiently close. The *d* and q-axis rotor flux components are shown in Fig. 7(c), which reflects flux orientation. The decoupling between flux and torque can be observed in Fig. 7(d).

D. Ramp Response

The ramp response of speed estimator is shown in Fig. 8. The reference speed (ω_r^*) is gradually changed from 0 to 30 rad/s following a ramp. The speed is maintained constant from 10 to 15 s. At 15 s, a negative ramp is applied. The motor speed is held constant at −30 rad/s after 25 s. The reference and actual rotor speeds are shown in Fig. 8(a). The actual and estimated speeds are shown in Fig. 8(b), which shows negligible speed estimation error. Flux orientation is well maintained as shown in Fig. 8(c).

E. Low-Speed Response

Low-speed operation is tested through a step command. The reference speed (ω_r^*) is changed from 0 to 5 rad/s. The actual speed (ω_r) is shown in Fig. 9(a). The actual and estimated ($\hat{\omega}_r$) speeds are presented in Fig. 9(b). The corresponding *d*- and q-axis rotor fluxes are shown in Fig. 9(c).

F. Performance Under the Variation of Stator Resistance

Here, the stator resistance is changed from its original values to twice the original value following a ramp [see Fig. 10(d)].

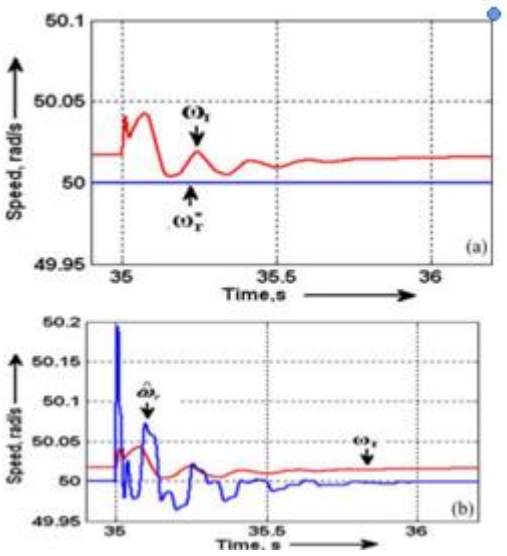

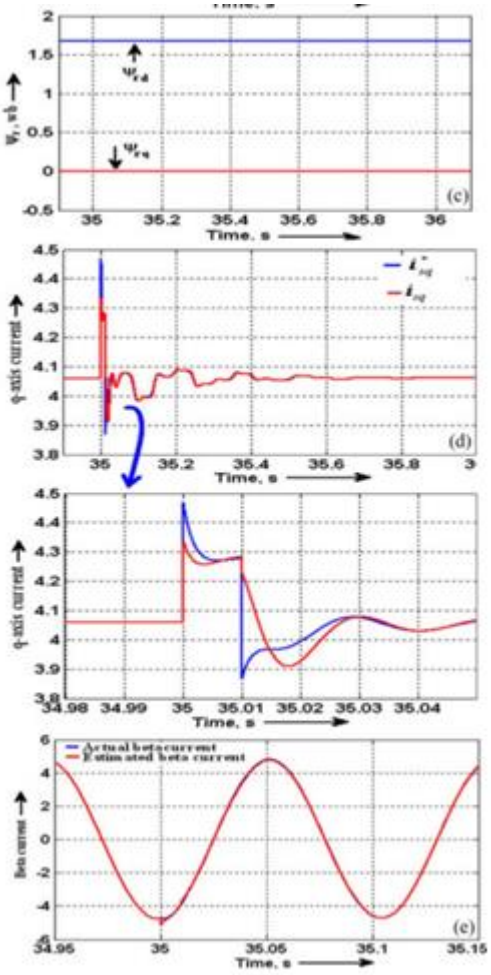

Fig. 5. Performance of the current estimation mechanism when subjected to a disturbance (as explained in Fig. 4) (a) reference and actual rotor speed (b)actual and estimated rotor speed (c) rotor flux (d) *q* axis current (e) actual and estimated β -axis current.

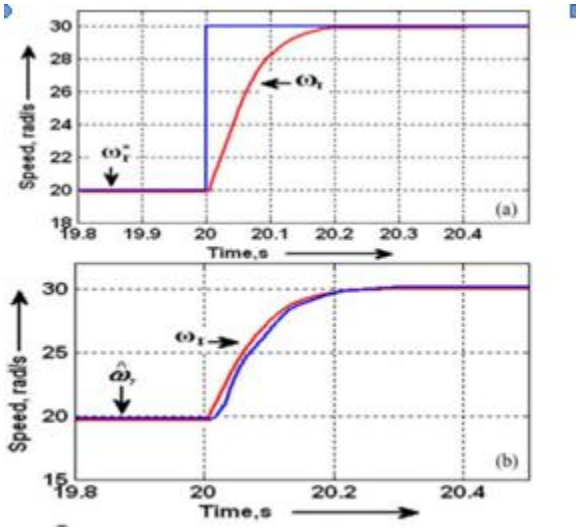

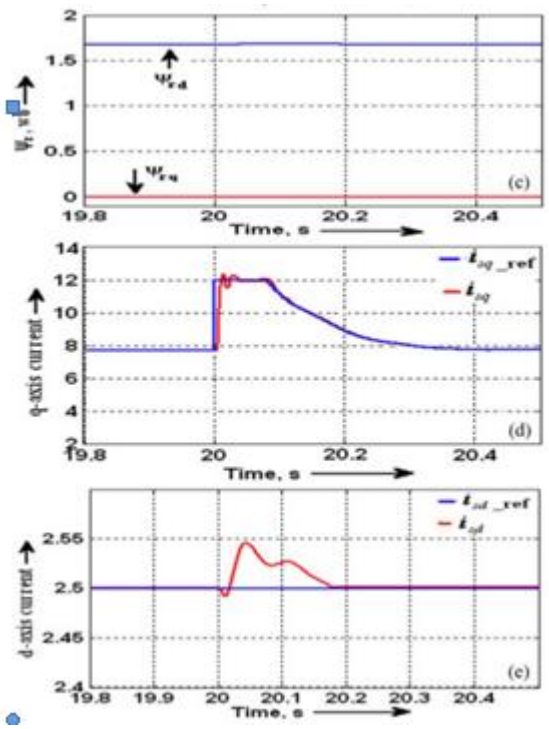

Fig. 6. Simulation results for step change in rotor speed (T_L = 1 p.u.): (a)reference and actual rotor speed, (b) actual and estimated rotor speed, (c) rotor flux, (d) *q*-axis current, and (e) *d*-axis current.

Reference speed is changed from 0 to 10 rad/s as shown in Fig. 10(a). It is observed from the figure that actual speed follows the reference speed. The system operates very well when subjected to such stator resistance variation [see Fig. 10(b)]. Fig. 10(c) confirms the orientation of flux.

G. Regenerating Mode of Operation

Performance of the system under regenerative mode of oper-ation is shown in Fig. 11. Here, the reference speed is changed

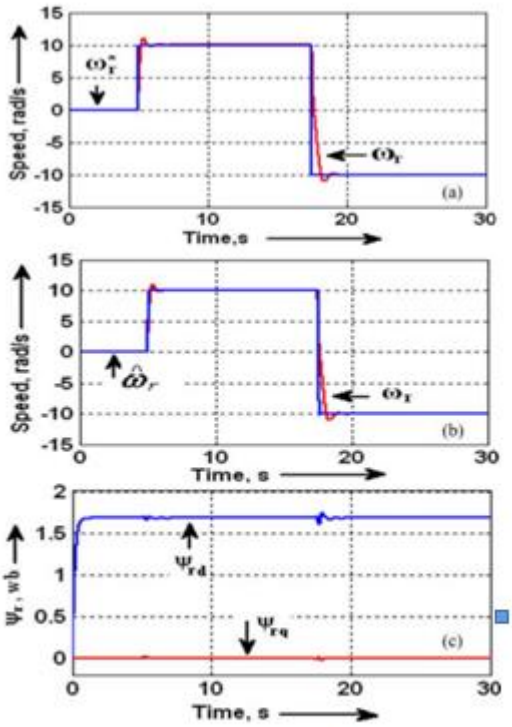

Fig. 7. Simulation results under speed reversal (*TL* = 0.5 p.u. at 10 rad/s): (a) reference and actual rotor speed, (b) actual and estimated rotor speed, and (c) rotor flux.

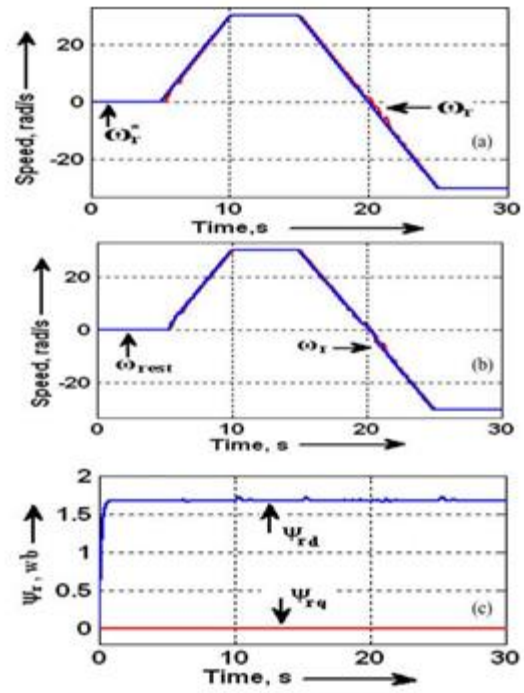

Fig. 8. Simulation results under ramp response (*TL* = 0.5 p.u. at 30 rad/s): (a) reference and actual rotor speed, (b) actual and estimated rotor speed, and (c) rotor flux.

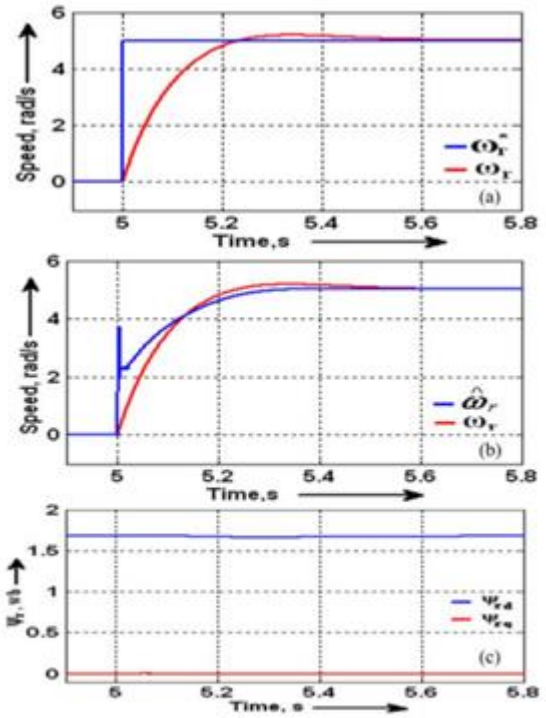

Fig. 9. Simulation results under low speed (TL = 0.5 p.u. at 5 rad/s): (a) reference and actual rotor speed, (b) actual and estimated rotor speed, and (c) rotor flux.

from 10 to −10 rad/s keeping the load torque positive (T_L = 5 N-m). The actual and reference speeds are shown in Fig. 11(a). Fig. 11(b) shows the estimated and actual speeds. Flux orien-tation can be seen in Fig. 11(c). The applied load torque and machine torque can be seen in Fig. 11(d).

H. Current Estimation at 20 and 5 rad/s

The performance of current estimator under step change in rotor speed command is shown in Fig. 12. Fig. 12(a) shows the actual and estimated β-axis current when the rotor speed is changed from 0 to 20 rad/s at 5 s. It can be observed from Fig. 12 that estimated current follows the actual current with good accuracy in steady state. Similar result is also obtained for speed change from 0 to 5 rad/s.

I. Performance Under the Variation of Rotor Resistance

It is important to see the performance of the drive in case of variation in rotor resistance. Here, the rotor resistance is changed from its actual value to 1.5 times the actual value in the form of step [see Fig. 13(e)]. Step change is considered such that it can be confirmed by experimentation as presented in Section VI. Reference speed is changed from 0 to 20 rad/s as shown in Fig. 13(a) and the load torque is set at 0.5 p.u. While estimated speed is again matching with the reference speed, the actual speed has now changed significantly. However, the

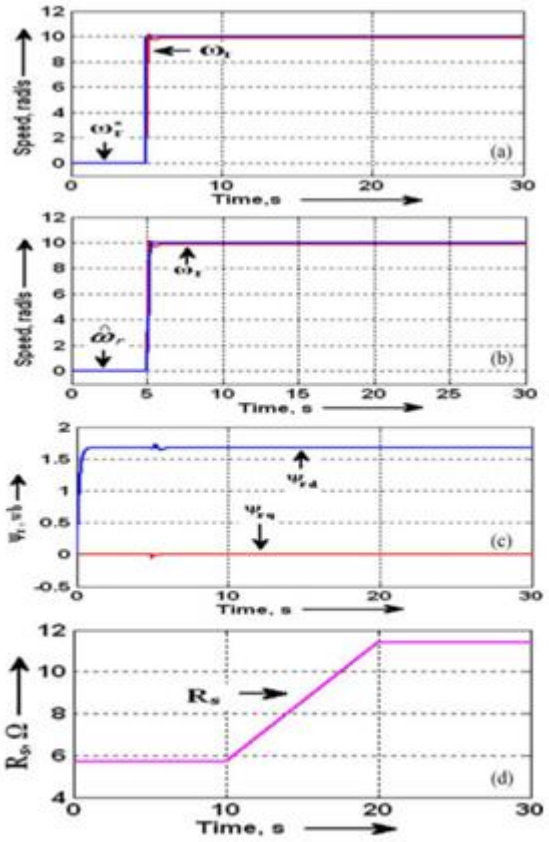

Fig. 10. Simulation results under variation in stator resistance: (a) reference and actual rotor speed, (b) actual and estimated rotor speed (c) rotor flux, and (d) variation of stator resistance.

current estimation [see Fig. 13(d)] and flux orientation [see Fig. 13(c)] remained satisfactory. Here, flux is calculated using current model with actual magnitudes of speed, currents, rotor parameters, and ω_e fed to motor by the controller.

J. Performance Under Field Weakening Region

It is clear from the overall block diagram (see Fig. 2) that neither the current estimation nor the speed estimation algo-rithms require a direct information of rotor flux as the flux is represented by the corresponding magnitude of $i_{s\,d}$. Hence, the magnitude of the rotor flux is decreased by reducing the d-axis stator current. A sample simulation result is presented in Fig. 14, which shows the performance of the drive under field weakening operation.

V. EXPERIMENTAL SETUP

This section deals with the development of laboratory proto-type. The test setup is built with the help of a dSPACE-

1104. The system shown in Fig. 15 has the following main units

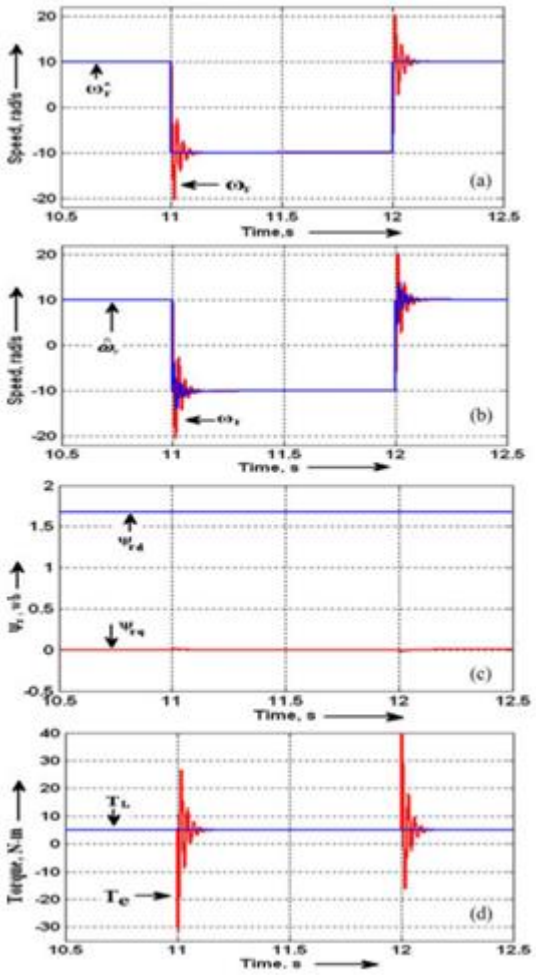

Fig. 11. Simulation results under motoring and regenerative mode of oper-ations (T_L = 5 N-m): (a) reference and actual rotor speed, (b) actual and estimated rotor speed, (c) rotor flux, and (d) electromagnetic torque and load torque.

A. Control Unit

The control unit operates through dSPACE-1104 controller board. The current is sensed and scaled before feeding to the controller. In case of any fault, the system has the debugging facility through a fault indication system. Control unit has the following functional blocks:

1. Sensing of phase current;
2. PWM processing block;
3. Protection and fault indication block; and
4. dSPACE-1104 controller board. *B. Power Unit*

This unit consists of the following modules.

1. Three-phase rectifier;
2. Voltage source inverter.

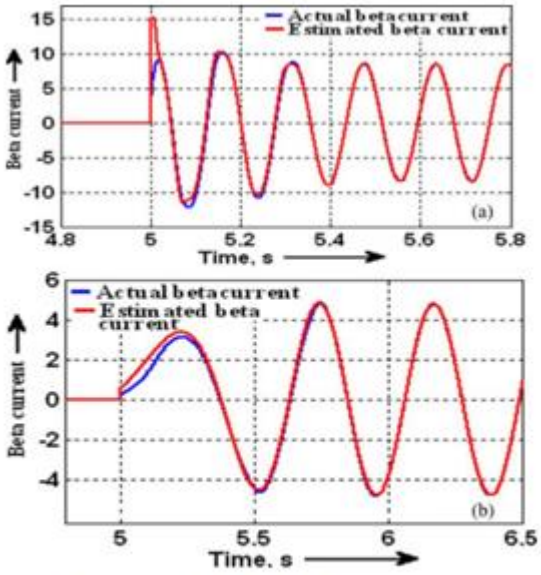

Fig. 12. Simulation results for step change in rotor speed: (a) actual and estimated β -axis current at 20 rad/s (TL = 1 p.u.), (b) actual and estimated β-axis current at 5 rad/s (TL = 0.5 p.u.).

The dSPACE-1104 controller board consists of a power PC and a slave DSP. The ADC, DAC, and the dedicated I/O ports are available within the power PC. The slave DSP provides the three output channels for three-phase PWM generation that are fed to the gate driver of the inverter through a PWM processing card. The control algorithms (e.g., speed estimation and cur-rent estimation) are developed in a real time platform, based on control-desk 5.3 software. The motor current is sensed through Hall-effect current sensors (LA-55P) and is given to the con-troller board with the help of ADC. A fault indication card is placed, which indicates the occurrence of overcurrent fault and generates signal to block the PWM pulses. A tacho-generator is mounted on the shaft of the motor for speed measurement. Tacho-generator gives the voltage signal, which is proportional to the speed of motor. Tacho-generator generates 3 V dc at 1000 r/min with a maximum speed of 4000 r/min. The tacho-generator is only used to check the actual speed of the motor. The speed loop is completed with the estimated speed.

VI. EXPERIMENTAL RESULTS

The proposed single-current-sensor-based speed sensorless algorithm is tested in hardware using the prototype, as discussed in the previous section. Some experimental results are presented in this section considering the current sensor to be in one of the phases (say in phase-A).

A. Step Response

The reference speed is changed from 0 to 20 rad/s at 9.5 s. The actual speed is shown in Fig. 16(a). The actual (ω_r) and estimated ($\omega\hat{}_r$) speeds are shown in Fig. 16(b). The flux orien-tation is well maintained as observed in Fig. 16(c). The applied load torque is 0.5 p.u. at 20 rad/s.

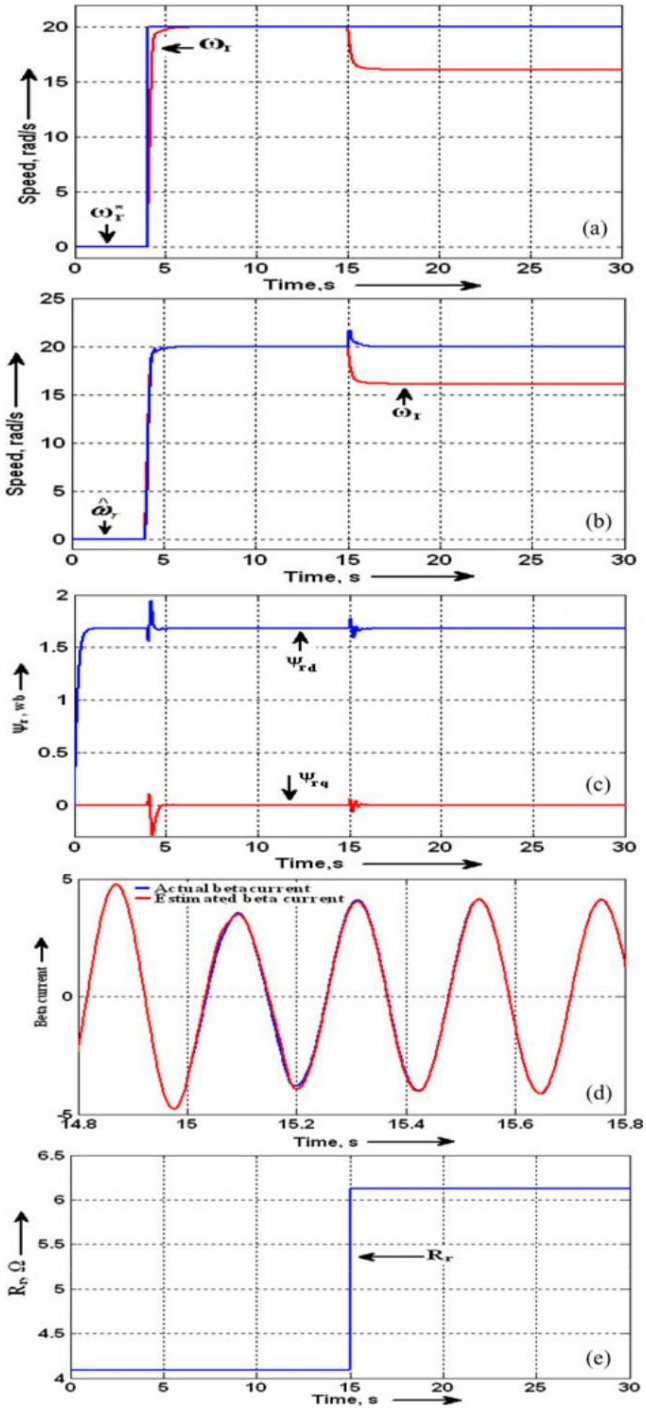

Fig. 13. Simulation results under step change in rotor resistance: (a) reference and actual rotor speed, (b) actual and estimated rotor speed, (c) actual rotor flux, (d) β -axis current, and (e) step change in rotor resistance.

B. Speed Reversal in Step

The performance of the drive is experimentally verified at speed reversal and the results are presented in Fig. 17. The reference versus actual and actual versus estimated speed are shown in Fig. 17(a) and (b), respectively.

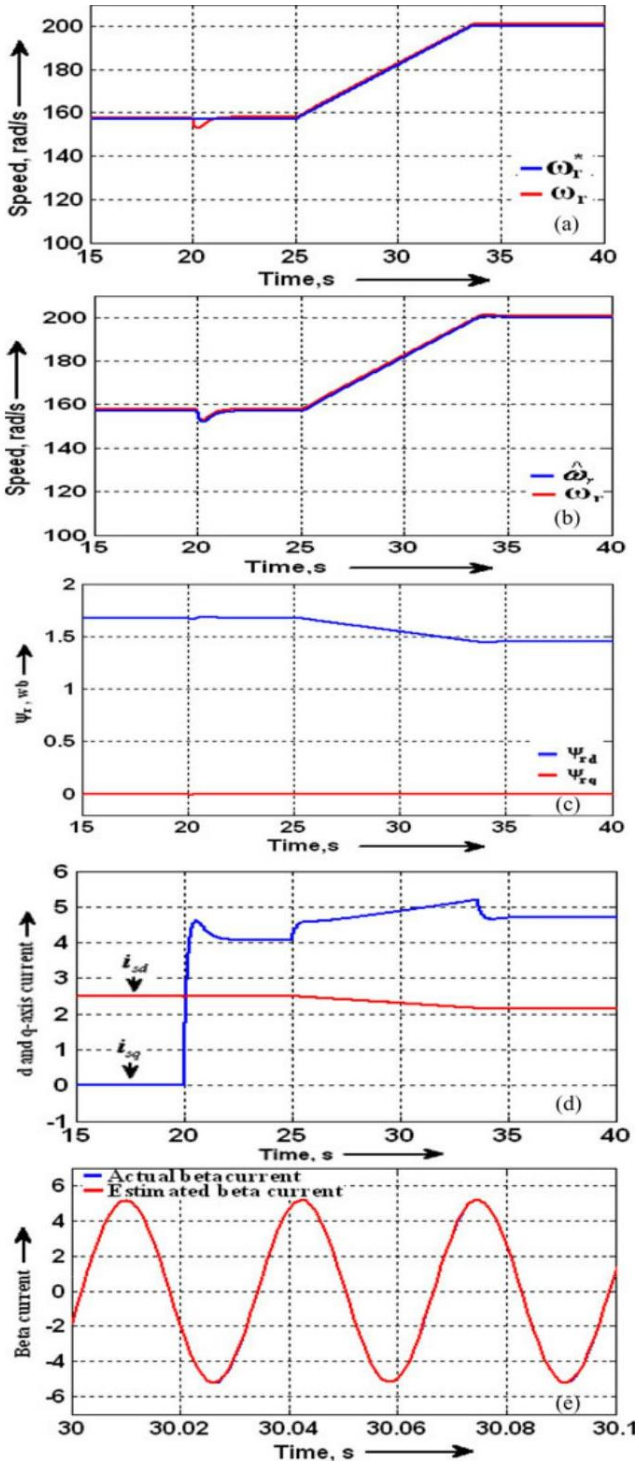

Fig. 14. Simulation results under field weakening region: (a) reference and actual rotor speed, (b) actual and estimated rotor speed, (c) rotor flux, (d) *d* and q-axis stator current, and (e) β -axis current.

C. Ramp Response

Performance of the system for a ramp speed command is shown in Fig. 18. The actual speed tracks the reference speed [see Fig. 18(a)]. The estimated speed is close to the actual speed, as observed in Fig. 18(b). The flux orientation is maintained, as shown in Fig. 18(c).

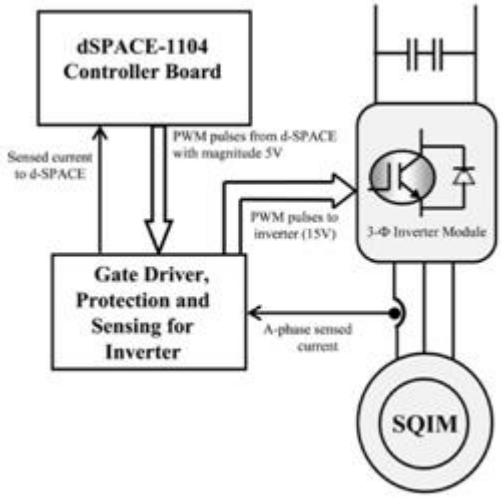

Fig. 15. Configuration of the experimental setup.

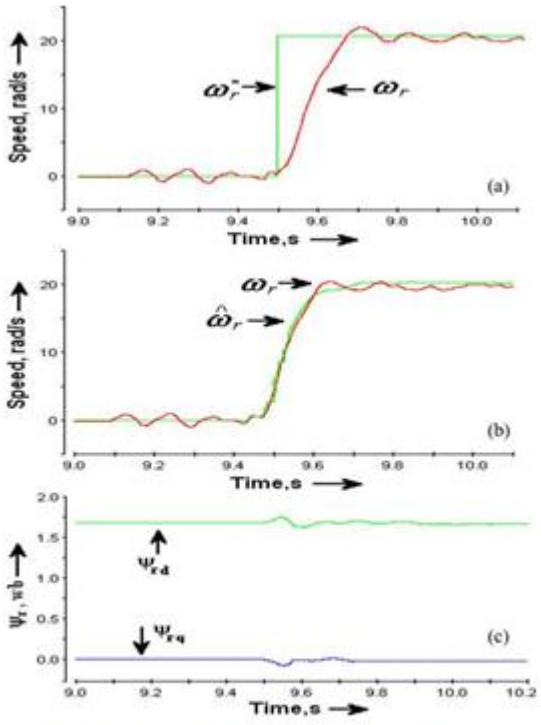

Fig. 16. Experimental results for step change in rotor speed (*TL* = 0.5 p.u. at 20 rad/s): (a) reference and actual rotor speed, (b) actual and estimated rotor speed, and (c) rotor flux.

D. Low-Speed Response

The hardware result corresponding to the operation of the system at 5 rad/s (reference speed) is shown in Fig. 19. Reference and actual speeds are shown in Fig. 19(a). Fig. 19(b) shows thatthe estimated speed matches with the actual speed satisfactorily.

The flux is oriented as seen from Fig. 19(c).

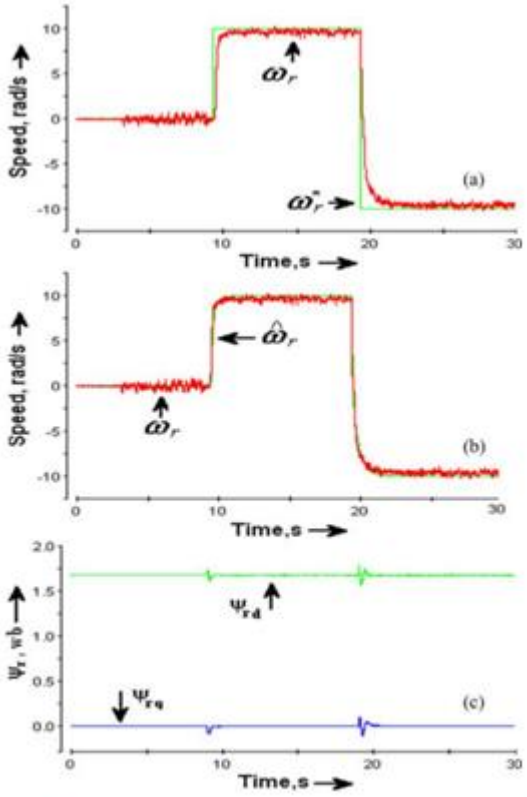

Fig. 17. Experimental results for speed reversal (*TL* = 0.5 p.u. at 10 rad/s): (a) reference and actual rotor speed, (b) actual and estimated rotor speed, and (c) rotor flux.

E. Performance Under the Variation of Rotor Resistance

As a slip-ring-type IM is used for experimentation, the perfor-mance of the drive for a variation of rotor resistance is checked by adding external resistance in the rotor circuit by a switch. Three equal resistances of magnitude half the value of the ro-tor resistance are connected in star. This is then connected to the three rotor terminals using a double pole double through switch. Initially all the three external resistances are shorted and at time 12.17 s, these are connected to the rotor remov-ing the short. Thus, there is no open-circuit condition when the external resistances are added to the rotor circuit. Hard-ware results corresponding to step change in rotor resistance is presented in Fig. 20. A variation similar to that observed in simulation [see Fig. 13(a)] is noted in actual value of speed [see Fig. 20(a)]. Estimated value of speed follows the reference speed [see Fig. 20(b)]. *q*-axis current is

presented in Fig. 20(c). From Fig. 20(d), it is confirmed that the estimated value of β-axis current matches well with the corresponding actual current. This proves the effectiveness of the current estimation technique in case of variation of rotor resistance.

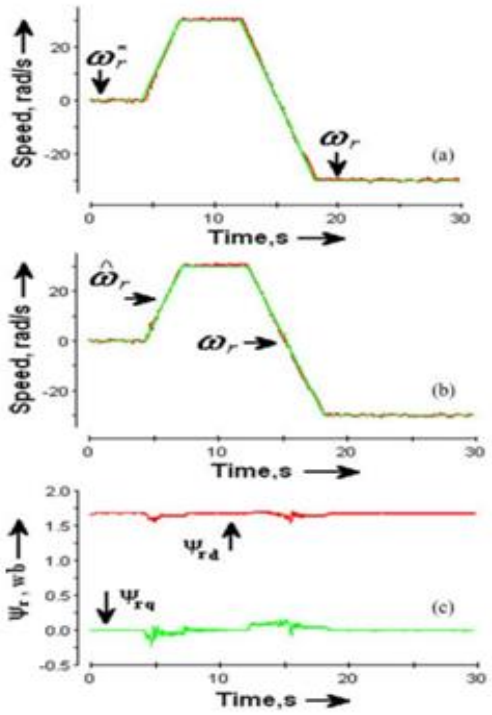

Fig. 18. Experimental results under ramp response (TL = 0.5 p.u. at 20 rad/s): (a) reference and actual rotor speed, (b) actual and estimated rotor speed, and (c) rotor flux.

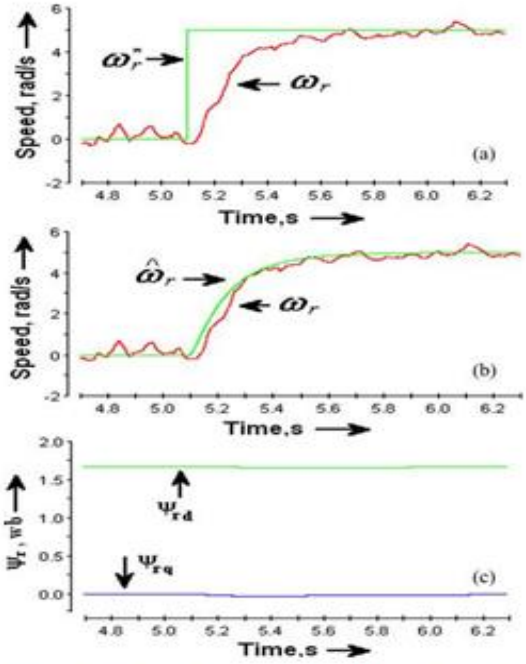

Fig. 19. Experimental results under low speed (TL = 0.5 p.u. at 5 rad/s): (a) reference and actual rotor speed, (b) actual and estimated rotor speed, and (c) rotor flux.

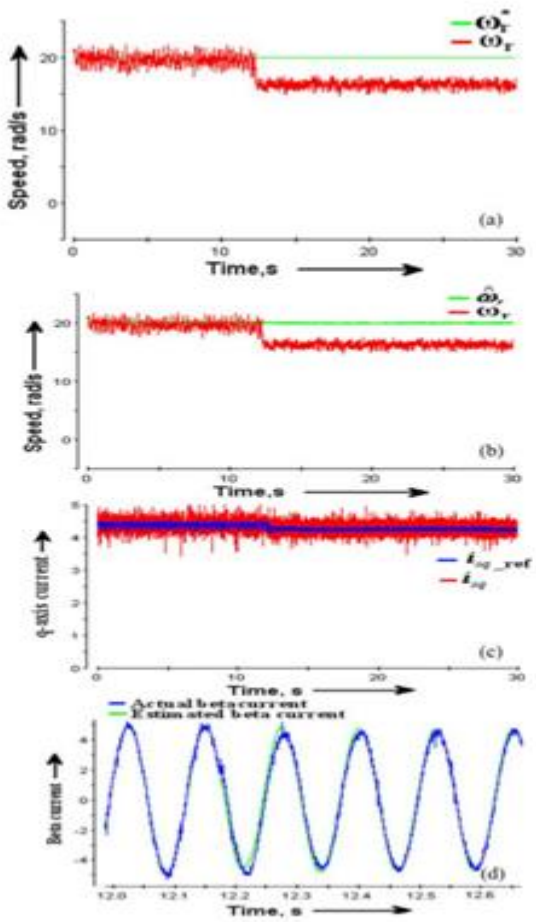

Fig. 20. Experimental results under step change in rotor resistance (T_L = 0.5 p.u. at 20 rad/s): (a) reference and actual rotor speed, (b) actual and estimated rotor speed, (c) q-axis current, and (d) actual and estimated β -axis current.

VII. CONCLUSION

A single current sensor-based vector controlled IM drive is presented in this paper. New techniques to estimate speed and current are utilized for the implementation. While the current estimation is based on the reference currents in synchronously rotating reference frame and the vector rotator, the speed estima-tion exploits a different form of X-MRAS. Both the techniques do not involve stator resistance. Hence, the proposed controller works very well at low speed. The proposed concept is ex-tensively simulated in MATLAB/Simulink. An experimental prototype is fabricated in the laboratory and the controllers are tested using dSPACE-1104-based controllers. The experimental results match very well with the simulation, which confirm the usefulness of the proposed low cost solution.

VIII. APPENDIX
CONTROLLER GAINS

Proportional gain of the speed controller	0.05
Integral gain of the speed controller	0.5
Proportional gain of the current controller	2.82
Integral gain of the current controller	571
Proportional gain of the MRAS adaptation mechanism	.1
Integral gain of the MRAS adaptation mechanism	9

IX. ACKNOWLEDGMENT

The authors would like to thank for the comments of anony-mous reviewers who have helped to improve the quality of the manuscript.

REFERENCES

[1] W. Leonhard, *Control of Electrical Drives*, 3rd ed. New Delhi, India: Springer, 2009.
[2] S. M. A. Cruz, "An active-reactive power method for the diagnosis of rotor faults in three-phase induction motors operating under time-varying load conditions," *IEEE Trans. Energy Convers.*, vol. 27, no. 1, pp. 71–84, Mar. 2012.
[3] G. Siraki and P. Pillay, "An in situ efficiency estimation technique for induction machines working with unbalanced supplies," *IEEE Trans. Energy Convers.*, vol. 27, no. 1, pp. 85–95, Mar. 2012.
[4] Bechouche, H. Sediki, D. O. Abdeslam, and S. Haddad, "A novel method for identifying parameters of induction motors at standhill using adaline," *IEEE Trans. Energy Convers.*, vol. 27, no. 1, pp. 105–116, Mar. 2012.
[5] S. C. Chang and S. N. Yeh, "Current sensorless field-oriented control of induction motors," *IEE Proc. Electr. Power Appl.*, vol. 143, pp. 492–500, 1996.
[6] S. Morimoto, M. Sanada, and Y. Takeda, "High-performance current-sensorless drive for PMSM and SynRM with only low-resolution position sensor," *IEEE Trans. Ind. Appl.*, vol. 39, no. 3, pp. 792–801, May/Jun. 2003.
[7] T. Matsuo and T. A. Lipo, "Current sensorless field oriented control of synchronous reluctance motor," *IEEE Ind. Appl. Soc. Annu. Meeting Conf. Rec.*, pp. 672–678, 1993.
[8] Schauder, "Adaptive speed identification for vector control of induction motors without rotational transducers," *IEEE Trans. Ind. Appl.*, vol. 28, no. 5, pp. 1054–1061, Sep./Oct., 1992.
[9] M. Rashed and A. F. Stronach, "A stable back-emf MRAS-based sen-sorless low speed induction motor drive insensitive to stator resistance variation," *IEE Proc. Electr. Power Appl.*, vol. 151, no. 6, pp. 685–693, 2004.
[10] J. Holtz, "Sensorless control of induction motor drives," *Proc. IEEE*, vol. 90, no. 8, pp. 1359–1394, Aug. 2002.